Title

Potent and Selective Double-Headed Thiophene-2-carboximidamide Inhibitors of Neuronal Nitric Oxide Synthase for the Treatment of Melanoma

Journal

Journal of Medicinal Chemistry, 57(3)

ISSN

0022-2623

Authors

Huang, He

Li, Huiying

Yang, Sun

et al.

Publication Date

2014-02-13

DOI

10.1021/jm401252e

Peer reviewed

Journal of Medicinal Chemistry

Article

pubs.acs.org/jmc

Potent and Selective Double-Headed Thiophene-2-carboximidamide Inhibitors of Neuronal Nitric Oxide Synthase for the Treatment of Melanoma

He Huang,[†] Huiying Li,[‡] Sun Yang,[§] Georges Chreifi,[‡] Pavel Martásek,[∥,⊥] Linda J. Roman,[∥] Frank L. Meyskens,[§] Thomas L. Poulos,*[,‡] and Richard B. Silverman*[,†]

[†]Department of Chemistry, Department of Molecular Biosciences, Chemistry of Life Processes Institute, Center for Molecular Innovation and Drug Discovery, Northwestern University, 2145 Sheridan Road, Evanston, Illinois 60208-3113, United States

[‡]Departments of Molecular Biology and Biochemistry, Pharmaceutical Sciences, and Chemistry, University of California, Irvine, California 92697-3900, United States

[§]Chao Family Comprehensive Cancer Center, University of California, Irvine, California 92697-3900, United States

[∥]Department of Biochemistry, University of Texas Health Science Center, San Antonio, Texas 78384-7760, United States

[⊥]Department of Pediatrics and Center for Applied Genomics, First School of Medicine, Charles University, Prague, Czech Republic

Supporting Information

ABSTRACT: Selective inhibitors of neuronal nitric oxide synthase (nNOS) are regarded as valuable and powerful agents with therapeutic potential for the treatment of chronic neurodegenerative pathologies and human melanoma. Here, we describe a novel hybrid strategy that combines the pharmacokinetically promising thiophene-2-carboximidamide fragment and structural features of our previously reported potent and selective aminopyridine inhibitors. Two inhibitors, **13** and **14**, show low nanomolar inhibitory potency (K_i = 5 nM for nNOS) and good isoform selectivities (nNOS over eNOS [440- and 540-fold, respectively] and over iNOS [260- and 340-fold, respectively]). The crystal structures of these nNOS−inhibitor complexes reveal a new hot spot that explains the selectivity of **14** and why converting the secondary to tertiary amine leads to enhanced selectivity. More importantly, these compounds are the first highly potent and selective nNOS inhibitory agents that exhibit excellent in vitro efficacy in melanoma cell lines.

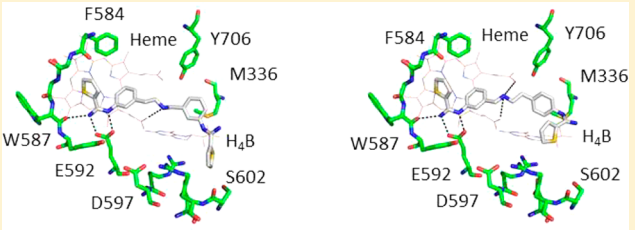

INTRODUCTION

Nitric oxide synthases (NOSs) are responsible for the biological production of nitric oxide (NO), an important second messenger that regulates many biological processes such as neurotransmission, vasodilation, and immune response.[1] NOSs catalyze two sequential reactions that convert L-arginine to L-citrulline and the free radical NO in the presence of oxygen and reduced nicotinamide adenine dinucleotide phosphate (NADPH) with N^{ω}-hydroxy-L-arginine (NHA) as an intermediate.[2−4]

There are three mammalian NOS isoforms: neuronal NOS (nNOS), inducible NOS (iNOS), and endothelial NOS (eNOS). All three isoforms are homodimers and share catalytic properties. However, according to various tissue distributions, NO generated from different NOS isoforms can play a wide range of physiological functions.[5,6] Overproduction of NO by nNOS has been implicated in many chronic neurodegenerative pathologies. Our previous studies have shown that NO from nNOS plays an important role in increasing the invasion and proliferation of human melanoma cells, suggesting that targeting NO signaling may facilitate therapy and prevention.[7] Although inhibition of nNOS activity is a promising strategy for the treatment of such diseases, inhibition of iNOS and eNOS, especially the latter, may cause undesired side effects.[8,9] Therefore, to precisely control biological processes and improve the safety profile, selective inhibition of nNOS over the other two isoforms is important for any potential therapeutic agent. The close similarity of active site structures in all three isoforms[10,11] presents a critical barrier to the design of selective nNOS inhibitors.

In our continuous efforts to develop nNOS selective inhibitors, we discovered a series of highly potent and selective nNOS small molecule inhibitors with a 2-aminopyridinomethyl pyrrolidine scaffold (Figure 1, **1** and **2**).[12−16] Some showed excellent potency (K_i < 10 nM) and excellent selectivity for nNOS over eNOS (>2500-fold) and iNOS (>700-fold). Moreover, we have found that the 2-aminopyridine moiety not only can make hydrogen bonds (H-bonds) with the active site glutamate (Glu592 in nNOS or Glu363 in eNOS) but also can hydrogen bond with the heme propionate in a conformation flipped 180°, depending on the chirality of the

Received: August 13, 2013
Published: January 21, 2014

   dx.doi.org/10.1021/jm401252e | J. Med. Chem. 2014, 57, 686−700

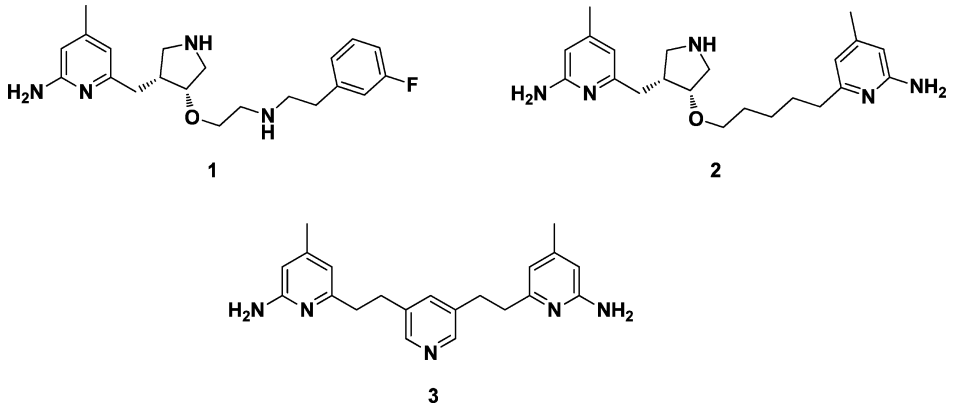

Figure 1. Chemical structures of **1**−**3**.

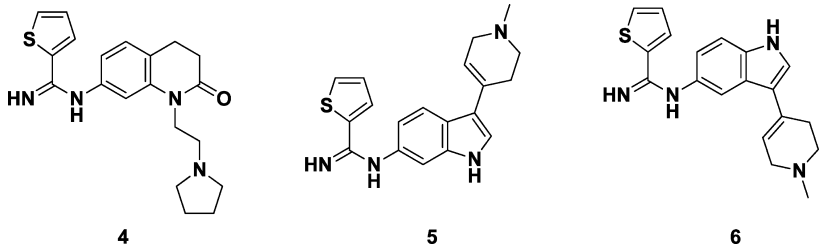

Figure 2. Chemical structures of **4**−**6**.

pyrrolidine. To achieve the two possible enzyme−inhibitor H-bonding interactions with a single compound and to simplify the synthetic routes, we developed a series of symmetric double-headed aminopyridines (e.g., **3** in Figure 1).[17,18] However, all of the aminopyridine-based inhibitors suffered from some limitations such as lack of oral bioavailability and/or poor membrane permeability. A fragment-based comparison of the in vitro enzyme assay versus the cellular assay clearly indicates that the aminopyridine moiety in these molecules may be an important factor that limits their membrane permeability.[19]

In addition to the aminopyridine-based inhibitors, thiophene-2-carboximidamides (Figure 2, **4**−**6**) represent another important class of nNOS inhibitors. Recently, some of these compounds were reported with promising pharmacological profiles.[20−25] Despite their favorable pharmacokinetics, they have significant challenges to overcome with respect to their lower potency and isozyme selectivities in vitro compared with the aminopyridine-containing inhibitors. In addition, few crystal structures depicting the binding mode of these molecules to the NOS isoforms have been reported; therefore, more crystallographic studies of thiophene-2-carboximidamides would be highly desirable.

Both the 2-aminopyridine and thiophene-2-carboximidamide moieties exhibit similar H-bond interactions with the enzyme, acting as mimics of the guanidinium group of the natural substrate L-Arg. Taken together, the thiophene-2-carboximidamide fragment would serve as a bioisostere of the 2-aminopyridine fragment with the potential for improved pharmacological profiles. Here we adopted a hybrid strategy and designed and synthesized a series of compounds that combines the thiophene-2-carboximidamide fragment and structural features of our potent and selective double-headed aminopyridine inhibitors (Figure 3). Furthermore, we conducted crystallographic studies to identify the inhibitor−enzyme interactions that promote nNOS-specific inhibition.

CHEMISTRY

The synthesis of **7** began with 1-iodo-3-nitrobenzene (Scheme 1). Homocoupling of 1-iodo-3-nitrobenzene gave **18** in a moderate yield. The nitro groups of **18** were reduced to amino groups in a quantitative yield, and then coupling with methyl thiophene-2-carbimidothioate hydroiodide salt was used to generate final product **7**. The coupling reaction of 3,3′-methylenedianiline with methyl thiophene-2-carbimidothioate hydroiodide salt gave final product **8**.

A synthetic route for target molecule **9** is shown in Scheme 2. Wittig reaction of 3-nitrobenzaldehyde with the corresponding phosphorus ylide of 1-(bromomethyl)-3-nitrobenzene allowed the isolation of the intermediate alkene in an 87% yield. Compound **23** was obtained by reduction of **21**, followed by treatment with methyl thiophene-2-carbimidothioate hydroiodide salt. Catalytic hydrogenation of **23** reduced the double bond, giving final product **9** in a high yield.

Nucleophilic addition of 3-nitrophenol with 2-bromo-1-(3-nitrophenyl)ethanone yielded **24** (Scheme 3). The carbonyl group of **24** was reduced to a hydroxyl group. Reduction of **25** gave **26**, which was allowed to react with methyl thiophene-2-carbimidothioate hydroiodide salt to give **10**.

Inhibitors **11** and **12** were synthesized as illustrated in Scheme 4. Nucleophilic addition of 3-nitrophenol with the corresponding alkyl halides generated **27** and **28**. Their nitro groups were reduced to give intermediates **29** and **30**, which were subsequently coupled with methyl thiophene-2-carbimidothioate hydroiodide salt to give final products **11** and **12**, respectively.

To synthesize inhibitors **13**−**17** (Scheme 5), reductive amination of 3-nitrobenzaldehyde with the corresponding amines generated **34**−**36**. The amino groups of **34**−**36** were

dx.doi.org/10.1021/jm401252e | J. Med. Chem. 2014, 57, 686−700

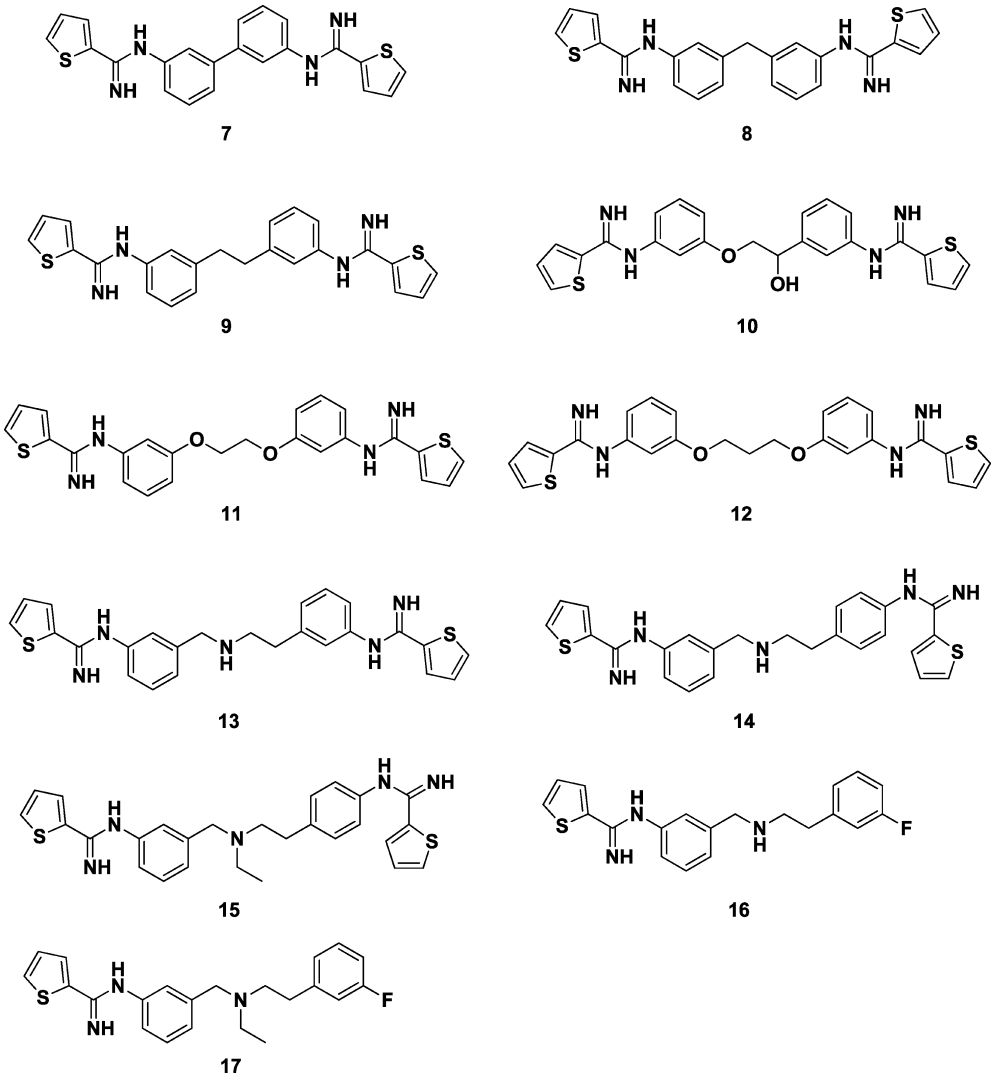

Figure 3. Target molecules designed and synthesized in this study.

protected with a Boc group. Reductive amination of **35** and **36** with acetaldehyde gave **40** and **41**, respectively. Amino group reduction and coupling with methyl thiophene-2-carbimidothioate hydroiodide salt were performed under conditions similar to those we adopted for the synthesis of **7**, giving target molecules **15**, **17**, and intermediates **47**–**49**. Deprotection of the Boc groups of **47**–**49** generated final products **13**, **14**, and **16**.

RESULTS AND DISCUSSION

Compounds **7**–**12** were designed with double thiophene-2-carboximidamide heads having diverse linkers. These flexible linkers mainly vary in length and, therefore, can provide precursor structural features that fit the enzyme active site appropriately. Table 1 shows the results of inhibition assays using purified NOS enzymes with **7**–**12**.

For this series, **7**–**10** display moderate inhibitory activity, while **11** and **12** are the best nNOS inhibitors. Compound **11** also shows outstanding nNOS selectivity over iNOS and good selectivity over eNOS. Compared to **11**, addition of one methylene group leads to a compound (**12**), with half the potency and a sharp decrease in selectivity for nNOS over both eNOS and iNOS.

To gain more insight into the structural basis for relative potencies and selectivities, we determined the crystal structure of several inhibitors bound to nNOS. The crystal structures revealed that **7** and **9** bind to nNOS as designed with one thiophene-2-carboximidamide head interacting with Glu592, while the other head occupies a hydrophobic pocket surrounded by Met336, Leu337, and Tyr706 near the active site entrance (Figure 4). The two phenyl rings in **7** are in van der Waals contacts with both heme propionates (Figure 4A). In contrast, having a 2-carbon linker between the two phenyl rings in **9** pushes the second phenyl and thiophene-2-carboximidamide head farther away from the heme (Figure 4B). The Leu337 side chain must adopt an alternate rotamer to accommodate lengthy compound **9**. The second carboximidamide in **9** does not make any direct contacts with the protein, while that in **7** makes only a weak H-bond with heme propionate D. Therefore, the submicromolar binding affinity is mainly attributed to the first phenyl ring and the thiophene-2-carboximidamide head that tightly anchors the inhibitor to the NOS active site. The structure of **10** bound to nNOS (data not shown) also supports this conclusion. While the first phenyl ring and thiophene-2-carboximidamide head is clearly shown in the electron density, the remainder of the compound is

dx.doi.org/10.1021/jm401252e | J. Med. Chem. 2014, 57, 686–700

Scheme 1. Synthesis of 7 and 8[a]

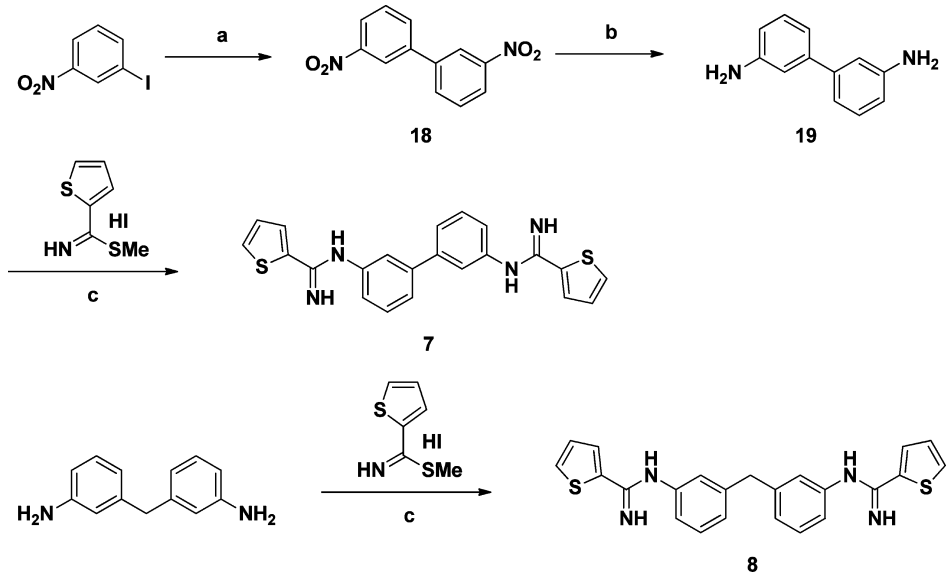

[a]Reagents and conditions: (a) $Pd_2(dba)_3$, tri(*o*-tolyl)phosphine, DIEA, 100 °C, 8 h, 61%; (b) Raney Ni, hydrazine hydrate, room temp, 30 min, quantitative; (c) EtOH, room temp, 24 h, 54−58%.

Scheme 2. Synthesis of 9[a]

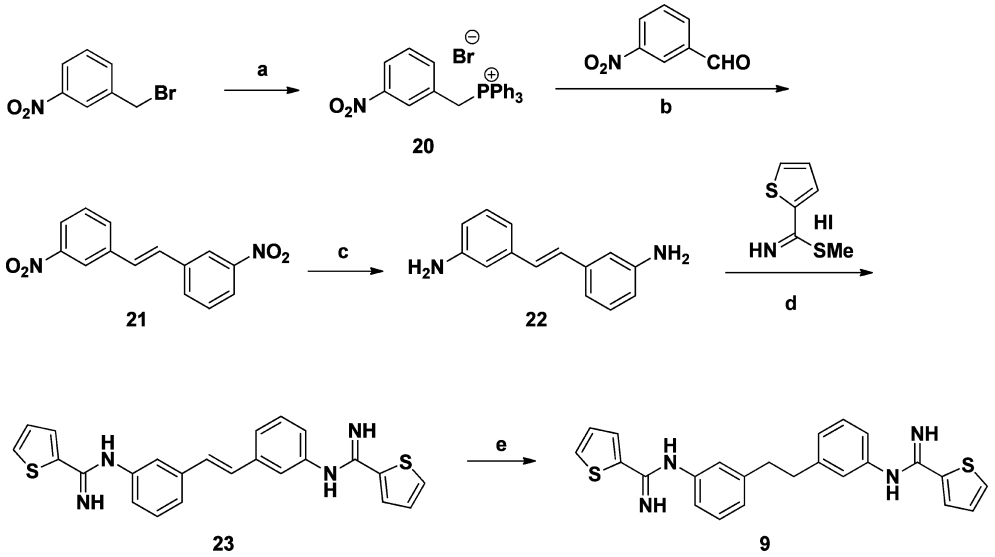

[a]Reagents and conditions: (a) PPh_3, toluene, 90 °C, 12 h, 97%; (b) LHMDS, THF, −78 °C to room temp, 4 h, 87%; (c) Raney Ni, hydrazine hydrate, room temp, 30 min, quantitative; (d) EtOH, room temp, 24 h, 46%; (e) H_2, Pd/C, EtOH, room temp, 24 h, 91%.

disordered. Nevertheless, **10** shares a similar affinity to nNOS as **7** and **9** (Table 1).

Compounds with a longer (4- or 5-atom) linker between the two head groups, **11** and **12**, exhibit much improved potency (Table 1). The **11**-nNOS structure (Figure 5A) provides an explanation. Similar to the cases of **7** and **9**, one phenyl ring and the thiophene-2-carboximidamide head of **11** recognizes the nNOS active site and H-bonds to Glu592 with the carboximidamide nitrogens. The O atom in the central linker distal to the active site forms a weak H-bond (3.4 Å) with Gln478. This brings the second phenyl ring next to Arg481. The Arg481 guanidinium plane has to rotate to make a better cation−aromatic stacking interaction with the phenyl ring of **11**. In addition, the N atom in the second head joins a H-bonding network involving Arg596, Asp600, and Arg603 via a water molecule. Interestingly, this thiophene-2-carboximidamide head reaches to a pocket surrounded by Trp306 (in the other subunit of the dimer), Asp600, Ser602, and Arg603 (Figure 5B). This is the first time we have found an inhibitor reaching into this pocket. Sequence alignment reveals that Ser602 in nNOS is a His or a Gln at the corresponding positions in eNOS and iNOS, respectively. It is likely that interactions between the thiophene-2-carboximidamide and this unique hot spot affects the selectivity of **11** while the extensive aforementioned enzyme−inhibitor interactions account for the better potency. Linker length also is quite important because increasing the linker by one atom in going from **11** to **12** results in a 2-fold lower potency. The **12**-nNOS structure (data not

dx.doi.org/10.1021/jm401252e | *J. Med. Chem.* 2014, 57, 686−700

Scheme 3. Synthesis of 10[a]

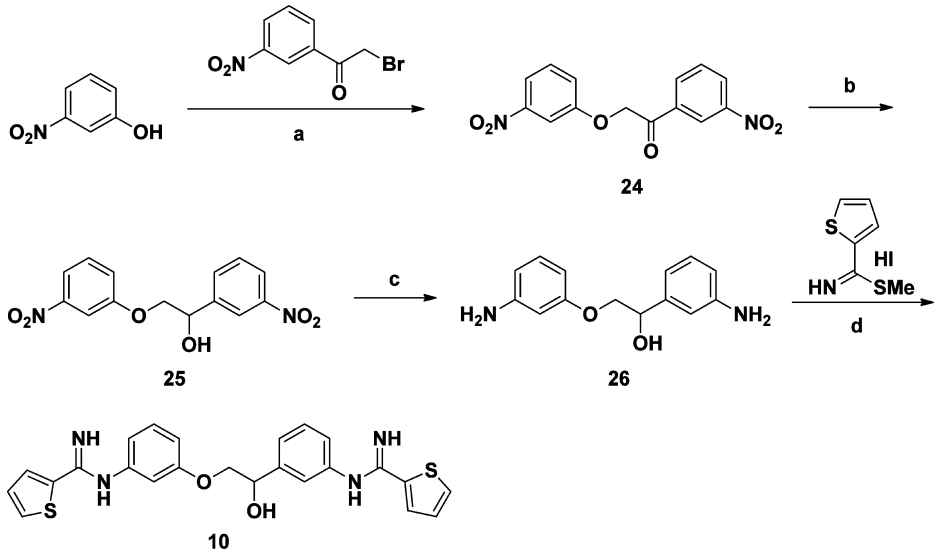

[a]Reagents and conditions: (a) K_2CO_3, DMF, room temp, 6 h, 73%; (b) $NaBH_4$, THF, room temp, 8 h, 80%; (c) Raney Ni, hydrazine hydrate, room temp, 30 min, quantitative; (d) EtOH, room temp, 24 h, 41%.

Scheme 4. Synthesis of 11 and 12[a]

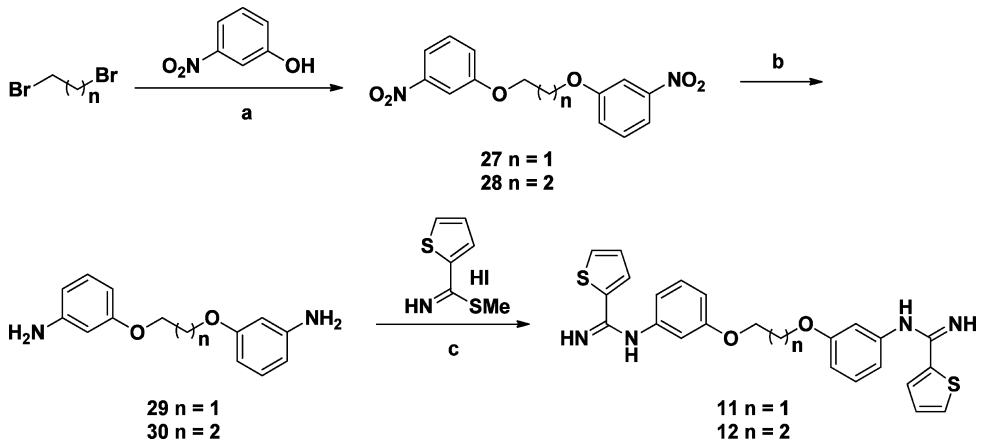

[a]Reagents and conditions: (a) K_2CO_3, DMF, 60 °C, 6 h, 71−80%; (b) Raney Ni, hydrazine hydrate, room temp, 30 min, quantitative; (c) EtOH, room temp, 24 h, 59−58%.

shown) shows that while the first phenyl ring and thiophene-2-carboximidamide head clearly bind to the nNOS active site similarly to that of **11**, the other head is too flexible to be modeled with certainty.

nNOS has two negative charges in the active site (Glu592 and Asp597) compared to one in eNOS (Glu363). As a result, nNOS provides better electrostatic stabilization for positively charged inhibitors. Inspired by our previously reported highly selective and potent pyrrolidine-containing nNOS inhibitors (**1** and **2**), we introduced a basic nitrogen atom mimicking the pyrrolidine N atom in the linker part of **11**, leading to **13** and **14**, to enhance the binding affinity and selectivity (Table 2). The results are impressive because both K_i values of **13** and **14** for nNOS are 5 nM, which is 25-fold more potent than that of **11**. Moreover, they display good selectivities of nNOS over iNOS and eNOS. The crystal structures of **13** and **14** bound to nNOS show that, as expected, both use the first phenyl ring and thiophene-2-carboximidamide head to anchor the inhibitor to the nNOS active site (Figure 6). The newly introduced amino group in the linker is situated between the two heme propionates. These electrostatic interactions are very likely the main source of binding affinity gained by the two compounds. However, **13** and **14** have a different phenyl ring in the second head. While **13** bears a meta-bisubstituted phenyl ring, the one in **14** is para-bisubstituted. The structural differences around the phenyl ring influence the way the second thiophene-2-carboximidamide headgroup interacts with the protein. The head in **13** reaches the same pocket next to Ser602 described for **11** but through a different "route". This is because the new inhibitor−heme electrostatic interactions direct the second phenyl ring of **13** to pack against Met336 (Figure 6A) rather than Arg481, as in the case of **11** (Figure 5A). The second thiophene-2-carboximidamide head in **14** is partially disordered because the para-bisubstituted phenyl forces the thiophene tail toward the position of Trp306 (in the other subunit). The tail has to make a sharp turn to avoid clashes (Figure 6B).

dx.doi.org/10.1021/jm401252e | J. Med. Chem. 2014, 57, 686−700

Scheme 5. Synthesis of 13−17[a]

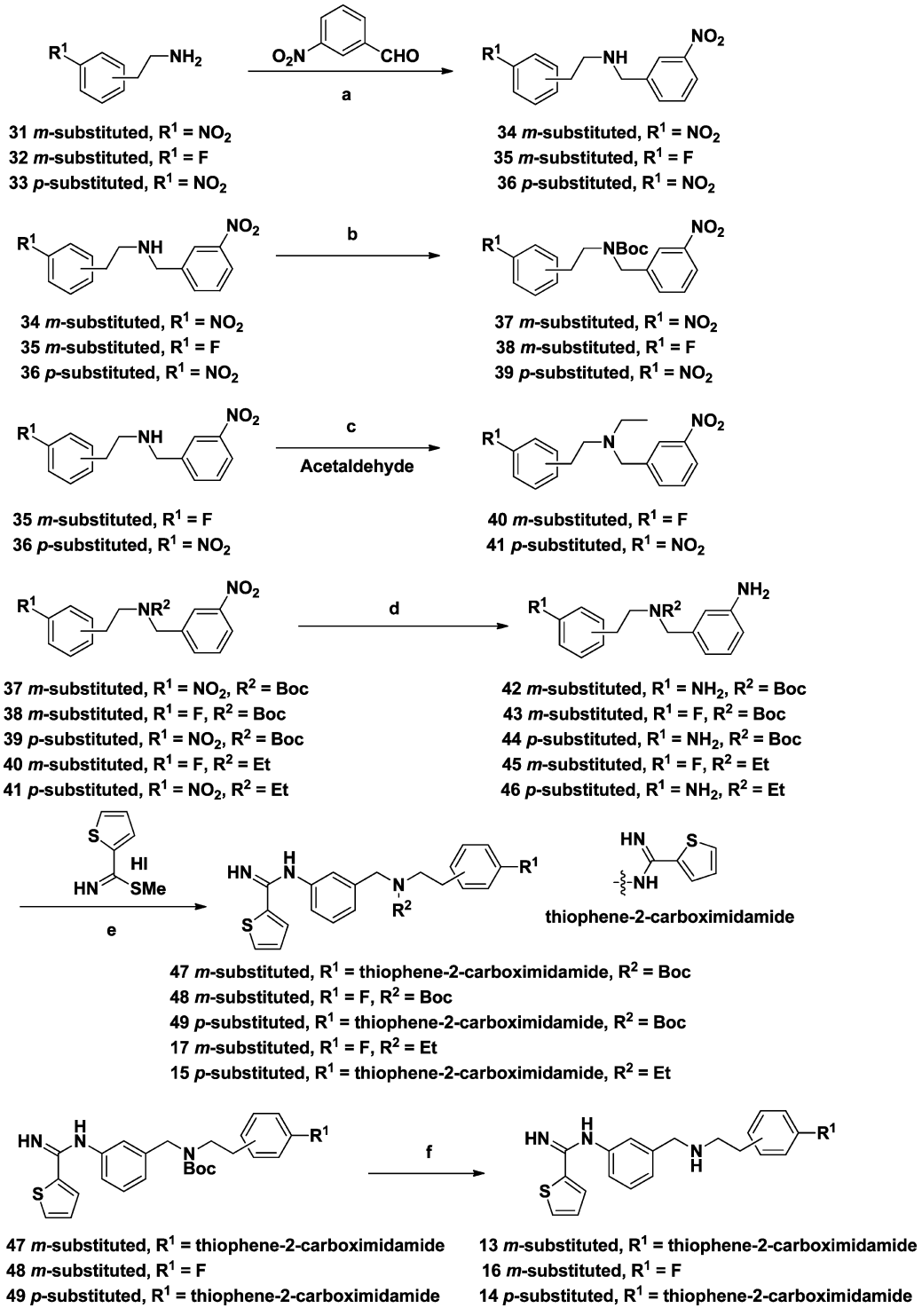

[a]Reagents and conditions: (a) Et_3N, $NaBH_3CN$, THF, room temp, 12 h, 69−72%; (b) $(Boc)_2O$, DMAP, MeOH, room temp, 12 h, 92−94%; (c) $NaBH_3CN$, THF, room temp, 12 h, 58−64%; (d) Raney Ni, hydrazine hydrate, room temp, 30 min, quantitative; (e) EtOH, room temp, 24 h, 48−53%; (f) 3N HCl/MeOH, room temp, 24 h, quantitative.

The basicity of the amine in the linker is important for potency, but this secondary amine is also a potential metabolic site that can be easily converted to a secondary hydroxylamine or serve as a substrate for flavin monooxygenases.[26] Therefore, we introduced a small ethyl group at the basic N atom of **14** to block this potential metabolic site. Such a substitution (**15**) decreases the potency (leading to an almost 10-fold drop in nNOS inhibition) but affords an increase in selectivity of nNOS over eNOS (845-fold). To our surprise, the **15**-nNOS structure reveals that **15** (Figure 6C) binds to nNOS in an orientation 180° flipped from that of **14** (Figure 6B). With **15**, it is the para-bisubstituted phenyl ring and its adjacent thiophene-2-carboximidamide that binds to Glu592. This orientation still allows a H-bond between the ethylated tertiary amine and

dx.doi.org/10.1021/jm401252e | J. Med. Chem. 2014, 57, 686−700

Table 1. Inhibition of NOS Isozymes by Synthetic Inhibitors 7–12[a]

compd no.	K_i (μM)			selectivity	
	nNOS	iNOS	eNOS	n/i	n/e
7	0.787 ± 0.061	66.4 ± 5.2	177.3 ± 10.9	84	225
8	0.776 ± 0.069	79.0 ± 4.0	133.0 ± 12.4	102	171
9	0.739 ± 0.053	103.8 ± 8.7	66.0 ± 5.8	141	89
10	0.819 ± 0.067	10.1 ± 0.9	5.2 ± 0.4	12	6
11	0.130 ± 0.062	66.8 ± 2.7	13.7 ± 0.7	513	105
12	0.237 ± 0.019	12.6 ± 0.8	4.0 ± 0.3	53	17

[a]The compounds were evaluated for in vitro inhibition against three NOS isozymes: rat nNOS, bovine eNOS, and murine iNOS. Considering that three NOS isozymes are isolated from three different species, the activity or selectivity of these compounds may differ in human NOS isozymes.[39]

heme propionate D. Inhibitor **14** is close to both heme propionates while **15** is close to only one, which may be the structural basis for why **14** is a more potent inhibitor. Nevertheless, the second phenyl ring and thiophene-2-carboximidamide head in **15** are quite well-defined, making van der Waals contacts with Met336, Leu337, and Trp306 (in the other subunit).

To understand isoform selectivity, we also determined the structures of **14**-eNOS and **15**-eNOS. As shown in Figure 7A, **14** anchors its meta-bisubstituted phenyl ring and the connected thiophene-2-carboximidamide head to the eNOS active site next to Glu363, which is the same interaction seen in the **14**-nNOS structure. The salt bridges from the secondary amine in the linker of **14** to both heme propionates also exist in eNOS, which affords a low micromolar binding affinity of **14** to eNOS (Table 2). However, the second phenyl and thiophene-2-carboximidamide head of **14** are less well-defined in eNOS. The residual electron density is nevertheless clear enough to indicate that the thiophene head steers away from the pocket where the same thiophene in **14**-nNOS establishes more favorable inhibitor–protein interactions. We hypothesize that the reason for this different binding preference stems from an amino acid variant, Ser602 in nNOS but His373 in eNOS. The bulkier His373 side chain in eNOS makes the pocket too shallow to accommodate the thiophene head of **14**.

The inhibitor binding mode observed in the **15**-eNOS structure (Figure 7B) is almost the same as that seen in the **15**-nNOS structure (Figure 6C). That is, the para-bisubstituted phenyl ring brings the thiophene-2-carboximidamide next to Glu363 on one end and the tertiary amine next to heme propionate D on the other end, for H-bonds. This means that the 845-fold selectivity of **15** for nNOS over eNOS (Table 2) is associated with how the tail end of the inhibitor extending out of the active site interacts with the protein. Unfortunately, the position of this thiophene ring is less certain because of poorer density in this region in both the **15**-eNOS and **15**-nNOS structures. Even so, there are sufficient sequence differences in this area to provide a possible explanation for selectivity. The main difference is that Met336 in nNOS is Val106 in eNOS. The second phenyl ring of **15** in eNOS makes van der Waals contacts with Val106 and Leu107, while the same group in nNOS contacts Met336 and Leu337. As a result, there is the potential for greater nonpolar interactions in nNOS. Another factor is the contacts between the thiophene ring and a Trp side chain (Trp306 in nNOS or Trp76 in eNOS). These contacts are closer in nNOS than those in eNOS.

Changing the secondary amine in **14** to a tertiary amino in **15** improves selectivity. To explore whether such substitution is effective in other cases, especially in mono-thiophene-2-carboximidamide nNOS inhibitors, we designed and synthesized **16** and **17** (Table 3). One thiophene-2-carboximidamide head was replaced by a fluorobenzene fragment because fluorine has been widely used to alter the pharmacokinetic properties and overall drug-like properties of compounds.[27] Compound **16** drops about half of the nNOS inhibitory activity compared to parent compound **14**, and selectivity also decreases sharply, especially over eNOS. However, addition of an ethyl group at the basic nitrogen of **16** further enhances the nNOS over eNOS selectivity although it decreases the potency (Table 3), which shows the same trend as **14** and **15**. The reason for decreased potency may be the shorter length, thereby preventing additional van der Waals contacts with the protein that are afforded by the longer thiophene-2-carboximidamide head in **14**. Detailed interactions of **16** and **17** are shown in Figure 8.

Indeed, the structure of **16**-nNOS (Figure 8A) reveals that apart from the common features of NOS active site recognition through the thiophene-2-carboximidamide head seen for other analogues, the fluorobenzene head of **16** interacts only with Trp306 (other subunit). Compound **17** shows ~7-fold lower potency than **16**, mainly because it maintains only one H-bond

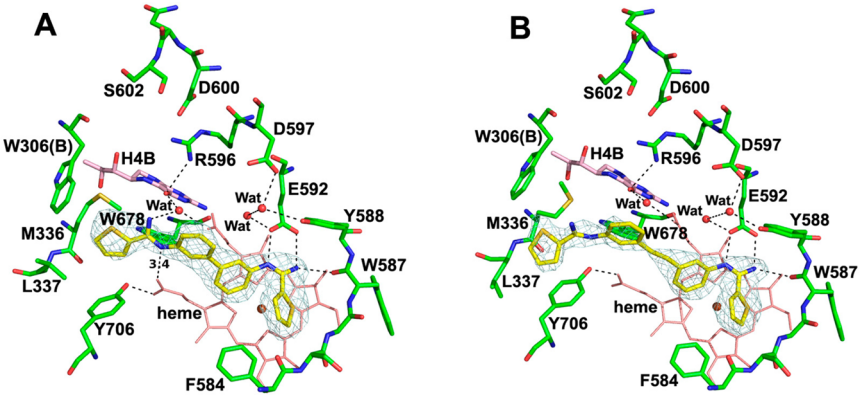

Figure 4. Crystallographic binding conformation of **7** (A) and **9** (B) in rat nNOS. The omit $F_o - F_c$ electron density maps for the inhibitors are shown at the 2.5 σ contour level. Relevant H-bonds are depicted with dashed lines. Key distances are labeled in Å. All structural figures were prepared with PyMol (www.pymol.org).

dx.doi.org/10.1021/jm401252e | J. Med. Chem. 2014, 57, 686–700

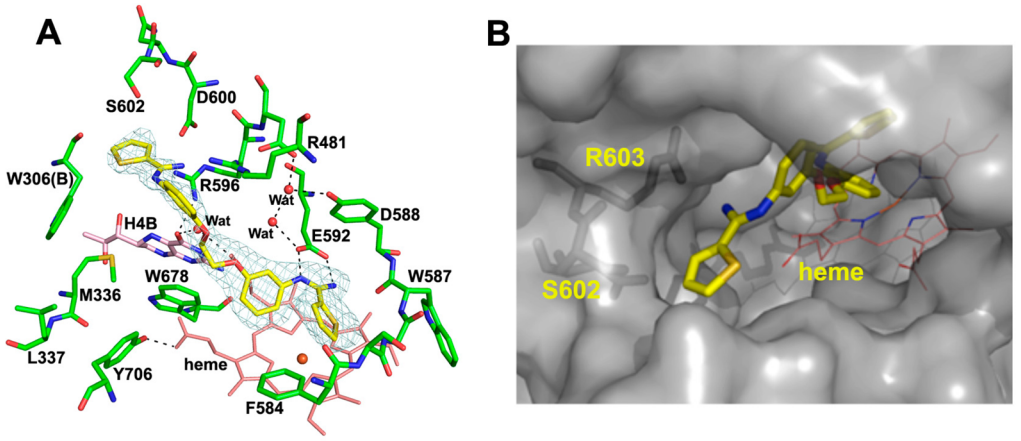

Figure 5. Crystallographic binding conformation of **11** with rat nNOS (A) and the new hot spot around the second thiophene head (B). The omit $F_o - F_c$ electron density maps for inhibitors are shown at the 2.5 σ contour level. Relevant H-bonds are depicted with dashed lines.

Table 2. Inhibition of NOS Isozymes by Synthetic Inhibitors 13−15[a]

	K_i (μM)			selectivity	
compd no.	nNOS	iNOS	eNOS	n/i	n/e
13	0.005 ± 0.0005	1.3 ± 0.2	2.2 ± 0.1	260	440
14	0.005 ± 0.0003	1.7 ± 0.1	2.7 ± 0.2	340	540
15	0.049 ± 0.002	14.2 ± 0.8	41.4 ± 2.2	290	845

[a]The compounds were evaluated for in vitro inhibition against three NOS isozymes: rat nNOS, bovine eNOS, and murine iNOS.

with heme propionate A via its tertiary amine (Figure 8B), while the secondary amine in **16** makes H-bonds/salt bridges with both heme propionates (Figure 8A). Moreover, the fluorobenzene in the **17**-nNOS complex has higher flexibility with weaker electron density, making a new hydrophobic interaction with Tyr706. This interaction forces the phenyl group of Tyr706 to rotate about 70° from what is seen in the **16**-nNOS structure. Although **17** is a weaker binder than **16**, the former has better selectivity (Table 3). The crystal structure shows that **16** (Figure 8C) binds to eNOS in an almost identical manner as that found in the **16**-nNOS structure (Figure 8A), and **17** also binds to eNOS (Figure 8D) similar to nNOS (Figure 8B). The only difference for **16** is the orientation of the F atom from fluorobenzene. In eNOS the F atom points toward Val106 and Leu107 for van der Waals contacts. To avoid clashes with the fluorobenzene of **16** (or **17**), the Tyr477 side chain rotates, as we observed with **17**-nNOS (Figure 8B). The subtle difference between **17**-eNOS (Figure 8D) and **17**-nNOS (Figure 8B) is also only in the position of fluorobenzene, which might be attributed to the amino acid variation in the vicinity. Met336 in nNOS is corresponds to Val106 in eNOS. Hydrophobic contacts (~3.5−3.9 Å) found between the fluorobenzene and Val106/Leu107 in **17**-eNOS are closer than those contacts (~4.3−4.8 Å) to Met336/Leu337 seen with **17**-nNOS. Although it is not clear that the differences near the tail end of the inhibitors is the explanation for isoform selectivity, it is clear that attaching an ethyl group to the secondary amine is a useful method to improve the nNOS/eNOS selectivity of these thiophene compounds.

Given the enzyme potency of **13** and **14**, we next tested whether these inhibitors were effective in melanoma cell lines. Detailed in our previous study,[7] nNOS is associated with the proliferation of melanoma and increased invasion, leading to subsequent development of metastases. nNOS inhibitors were able to efficiently inhibit melanoma proliferation and invasion with significant reduction of intracellular NO levels. Inhibitors **13** and **14** exhibited potent antimelanoma activity in vitro (Table 4). Their EC_{50} values in metastic melanoma A375 cells are 1.3 and 3.4 μM (Table 4), which is better than that of the chemotherapeutic drug cisplatin (4.2 and 14.3 μM in A375 and Sk-Mel28 cells, respectively).[7] Notably, the inhibition by **13** and **14** is more predominant in metastatic melanoma A375 cells compared to primary early stage Wm3211 cells, which supports our hypothesis that nNOS/NO signaling is more critical to melanoma progression than to the initiation phase. However, unexpectedly, these compounds also exhibited apparent inhibition of cell proliferation in primary normal cells, including melanocytes and fibroblast cells. Taken together, these results suggest that targeting nNOS provides a potential approach to block overactivated NO signaling in human melanoma.

CONCLUSIONS

In summary, we report the rational design of selective nNOS inhibitors using a hybrid strategy. Two compounds, **13** and **14**, show excellent potency (5 nM) and good selectivities for nNOS over the other isozymes. The crystal structures of these inhibitors bound to nNOS or eNOS have identified a new hot spot near Ser602 in nNOS (Figure 5B). The equivalent residue in eNOS is His373, which may be a contributing structural factor for the selectivity observed for **14** (Figure 6). A small ethyl substituent attached to the amine of the inhibitor acts as an important component for improving isoform selectivity. Importantly, **13** and **14** achieve good cellular activity in two melanoma cell lines. Altogether, these inhibitors are promising candidates for further development of improved therapeutics, and their structural features provide new clues for the future design and development of new selective nNOS inhibitors.

EXPERIMENTAL SECTION

All reagents were purchased from Sigma-Aldrich, Alfa Aesar, or TCI and were used without further purification unless stated otherwise. Analytical thin layer chromatography was visualized by ultraviolet light. Flash column chromatography was carried out under a positive pressure of air. ^{1}H NMR spectra were recorded on 500 or 400 MHz spectrometers. Data are presented as follows: chemical shift (in ppm on the δ scale, and the reference resonance peaks set at 0 ppm [TMS($CDCl_3$)] and 3.31 ppm (CD_2HOD), multiplicity (s = singlet, d

dx.doi.org/10.1021/jm401252e | J. Med. Chem. 2014, 57, 686−700

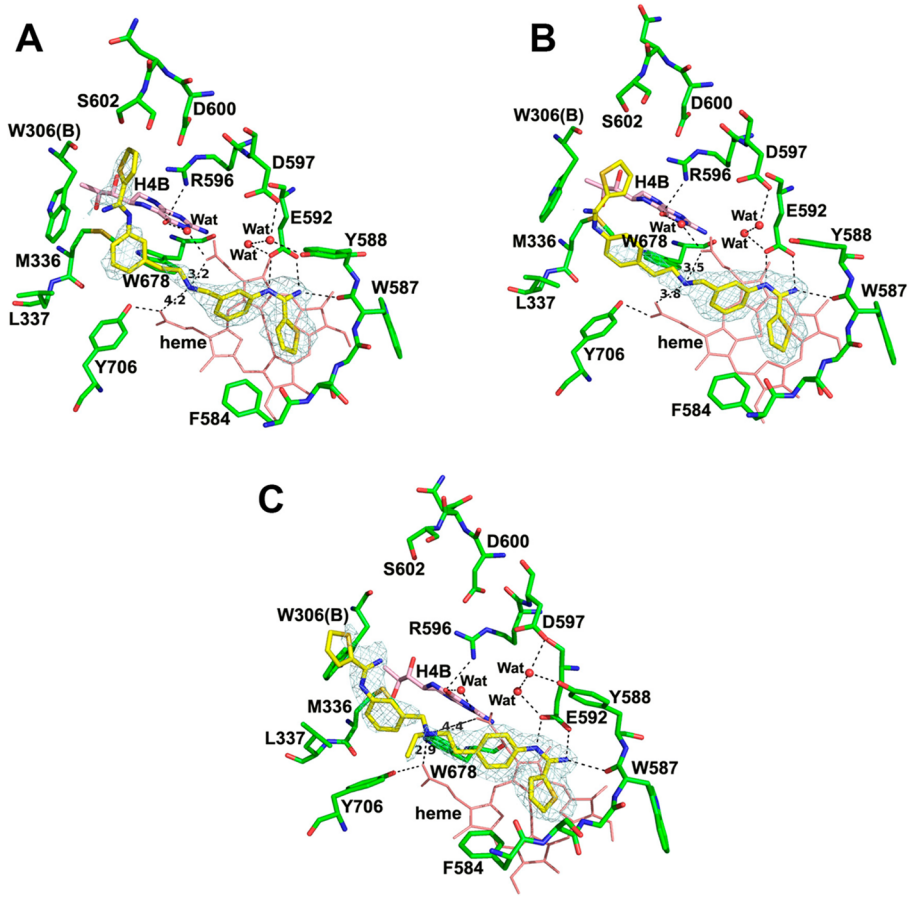

Figure 6. Crystallographic binding conformation of **13** (A), **14** (B), and **15** (C) with rat nNOS. The omit $F_o - F_c$ electron density maps for inhibitors are shown at the 2.5 σ contour level. Relevant H-bonds are depicted with dashed lines. Key distances are drawn with dashed lines and labeled in Å.

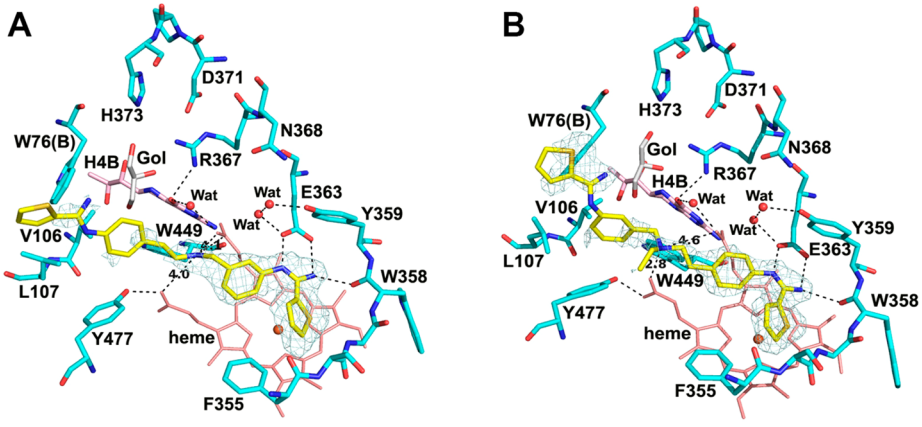

Figure 7. Crystallographic binding conformation of **14** (A) and **15** (B) with bovine eNOS. The omit $F_o - F_c$ electron density maps for inhibitors are shown at the 2.5 σ contour level. Relevant H-bonds are depicted with dashed lines. Key distances are drawn with dashed lines and labeled in Å.

= doublet, t = triplet, q = quartet, p = quintet, m = multiplet), coupling constant (J/Hz), and integration. ^{13}C NMR spectra were recorded at 125 or 100 MHz, and all chemical shift values are reported in ppm on the δ scale, with an internal reference of δ 49.0 for CD_3OD. High-resolution mass spectra were measured on liquid chromatography/time-of-flight mass spectrometry (LC-TOF). The purity of the tested compounds was determined by high-performance liquid chromatography (HPLC) analysis and was >95%.

General Procedure A: Nitro Group Reduction. To a solution of the reagent (1 mmol) in MeOH (10.0 mL) was added hydrazine hydrate (0.2 mL) and Raney nickel. The reaction mixture was stirred at room temperature for 30 min. Then the reaction mixture was filtered through Celite. The filtration was diluted with water, extracted with EtOAc, and washed with saturated $NaHCO_3$ and brine. The organic layer was concentrated in vacuo. The residue was purified by column chromatography to yield the product.

General Procedure B: Reductive Amination. To a solution of the aldehyde (1.0 mmol) and amine (1.0 mmol) in THF (20 mL) at 0 °C was added $NaBH_3CN$ (1.05 mmol) in three portions carefully. The reaction mixture was stirred at 0 °C for 30 min and then stirred overnight at room temperature. The reaction mixture was quenched with MeOH in an ice bath, extracted with EtOAc, and washed with

dx.doi.org/10.1021/jm401252e | J. Med. Chem. 2014, 57, 686−700

Table 3. Inhibition of NOS Isozymes by Synthetic Inhibitors 16 and 17[a]

compd no.	K_i (μM)			selectivity	
	nNOS	iNOS	eNOS	n/i	n/e
16	0.011 ± 0.001	1.6 ± 0.07	0.9 ± 0.05	145	82
17	0.073 ± 0.003	12.1 ± 0.74	21.7 ± 1.57	166	297

[a]The compounds were evaluated for in vitro inhibition against three NOS isozymes: rat nNOS, bovine eNOS and murine iNOS.

saturated $NaHCO_3$ and brine. The organic layer was concentrated in vacuo. The residue was purified by column chromatography to yield product.

General Procedure C: Boc-Protection. To a solution of the amine (1 mmol) in MeOH (15 mL) was added di-*tert*-butyl dicarbonate (1.2 equiv) and DMAP (cat.). The reaction mixture was stirred at room temperature for 12 h. Then the reaction mixture was concentrated in vacuo. The residue was purified by column chromatography to yield the product.

General Procedure D: Coupling Reaction of Amine with Methyl Thiophene-2-carbimidothioate Hydroiodide Salt. To a solution of the amine (1 mmol) in EtOH (15.0 mL) was added thiophene-2-carbimidothioate hydroiodide salt (1.5 equiv for monoamine and 3.0 equiv for diamine). The reaction mixture was stirred at room temperature for 36 h. Then the reaction mixture was concentrated in vacuo. The residue was purified by column chromatography to yield product.

General Procedure E: Boc-Deprotection. To a solution of the Boc-protected reagent (0.2 mmol) in MeOH (1.0 mL) was added 3N HCl (10.0 mL). The reaction mixture was stirred at room temperature for 24 h. Then the reaction mixture was concentrated in vacuo. The crude product was recrystallized with MeOH and cold diethyl ether to provide the product.

***N,N′*-([1,1′-Biphenyl]-3,3′-diyl)bis(thiophene-2-carboximidamide) (7).** To a solution of 1-iodo-3-nitrobenzene (3.0 mmol) in dry DIEA (20 mL) was added $Pd_2(dba)_3$ (0.05 equiv) and tri(*o*-tolyl)phosphine (0.1 equiv). The reaction mixture was stirred under argon at 100 °C for 8 h and then diluted with H_2O, extracted with EtOAc, and washed with water and brine. The organic layer was dried over Na_2SO_4 and concentrated in vacuo. The residue was purified by column chromatography to yield **18** (yield 61%). **7** was synthesized by general procedures A and D using **18** as the starting material (yield 54%). ^{1}H NMR (500 MHz, CD_3OD): δ 7.68 (d, J = 3.5 Hz, 2H), 7.60 (d, J = 5.0 Hz, 2H), 7.46 (t, J = 7.5 Hz, 2H), 7.40 (d, J = 7.5 Hz, 2H), 7.26 (s, 2H), 7.15 (dd, J = 5.0, 3.5 Hz, 2H), 7.00 (d, J = 7.5 Hz, 2H). ^{13}C NMR (125 MHz, CD_3OD): δ 156.61, 140.59, 135.37, 134.96, 134.59, 130.65, 129.07, 128.62, 126.63, 125.25, 124.12. LC-TOF ($M + H^+$) calcd for $C_{22}H_{19}N_4S_2$ 403.1046, found 403.1046.

***N,N′*-(Methylenebis(3,1-phenylene))bis(thiophene-2-carboximidamide) (8).** Compound **8** was synthesized by general procedure D using 3,3′-methylenediamiline as the starting material (yield 58%). ^{1}H NMR (500 MHz, CD_3OD): δ 8.10−8.00 (m, 4H), 7.53 (t, J = 7.5 Hz, 2H), 7.41−7.36 (m, 6H), 7.34 (d, J = 7.5 Hz, 2H), 4.18 (s, 2H). ^{13}C NMR (125 MHz, CD_3OD): δ 159.39, 144.70, 135.82, 135.50, 135.15, 131.76, 130.92, 130.30, 130.02, 127.25, 124.71, 41.99. LC-TOF ($M + H^+$) calcd for $C_{23}H_{21}N_4S_2$ 417.1202, found 417.1195.

***N,N′*-(Ethane-1,2-diylbis(3,1-phenylene))bis(thiophene-2-carboximidamide) (9).** LHMDS (1.0 M in THF, 2.4 mmol) was added to a suspension of **20** (2 mmol) in anhydrous THF (15 mL) at −78 °C. The reaction mixture was stirred under argon for 30 min, then warmed to 0 °C over 30 min. To this reaction mixture was added 3-nitrobenzaldehye (2.2 mmol) in anhydrous THF (3 mL) at −78 °C. The reaction mixture was warmed to room temperature and stirred for 4 h. The reaction mixture was then quenched with saturated NH_4Cl,

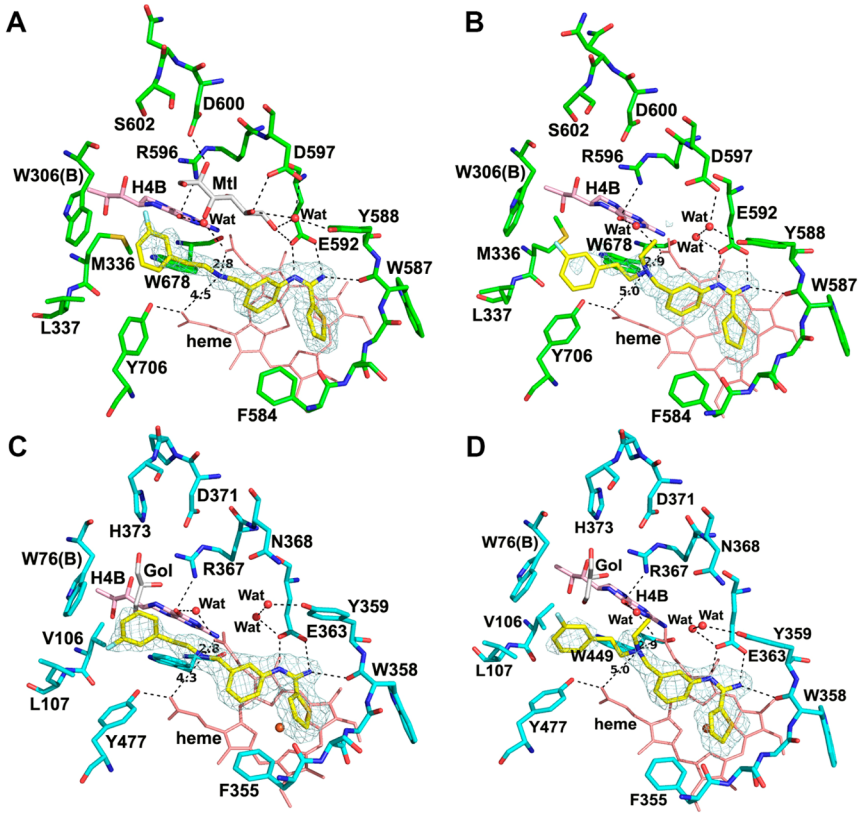

Figure 8. Crystallographic binding conformation of **16** (A) and **17** (B) with rat nNOS, as well as **16** (C) and **17** (D) with bovine eNOS. The omit $F_o - F_c$ electron density maps for inhibitors are shown at the 2.5 σ contour level. Relevant H-bonds are depicted with dashed lines. Key distances are drawn with dashed lines and labeled in Å.

dx.doi.org/10.1021/jm401252e | J. Med. Chem. 2014, 57, 686−700

Table 4. EC_{50} Values (μM) of 13 and 14 with Human Melanoma Cells

compd	primary melanoma wm3211 cell line	metastatic melanoma A375 cell line	primary fibroblast cells	primary keratinocytes	immortalized melanocytes
13	5.6	3.4	1.4	ND[a]	cannot calculate[b]
14	2.7	1.3	7.9	cannot calculate	cannot calculate

[a]Not done. [b]Toxic even at lower concentration and no dose−activity curve occurred.

extracted with EtOAc, and washed with water and brine. The organic layer was concentrated in vacuo. The residue was purified by column chromatography to yield **21** (yield 87%). Intermediate **24** was synthesized by general procedures A and D using **21** as the starting material (yield 46%). A solution of **24** (0.5 mmol) in MeOH (20 mL) was treated with 10% Pd/C (15 mg). The reaction mixture was stirred at room temperature under a hydrogen atmosphere for 24 h. The catalyst was removed by filtration through Celite, and the resulting solution was concentrated in vacuo. The crude material was purified by column chromatography to yield **9** (yield 91%). ^{1}H NMR (400 MHz, CD_3OD): δ 8.17−8.02 (m, 4H), 7.56−7.51 (t, J = 7.5 Hz, 2H), 7.45−7.38 (m, 6H), 7.36−7.30 (d, J = 7.5 Hz, 2H), 3.10 (s, 4H). ^{13}C NMR (100 MHz, CD_3OD): δ 156.90, 143.97, 136.57, 133.15, 132.73, 130.64, 129.92, 128.32, 128.26, 125.00, 122.43, 36.92. LC-TOF (M + H^+) calcd for $C_{24}H_{23}N_4S_2$ 431.1359, found 431.1359.

***N*-(3-(1-Hydroxy-2-(3-(thiophene-2-carboximidamido)-phenoxy)ethyl)phenyl)thiophene-2-carboximidamide (10).** To a solution of 3-nitrophenol (2 mmol) in DMF (20 mL) was added K_2CO_3 (2.2 mmol) and 2-bromo-1-(3-nitrophenyl)ethanone (2.2 mmol). The suspension was stirred for 6 h at room temperature. The reaction mixture was then diluted with H_2O (50 mL), extracted with EtOAc, and washed with water and brine. The organic layer was dried over Na_2SO_4 and concentrated in vacuo. The residue was purified by column chromatography to yield **24** (yield 73%). To a solution of **24** (1 mmol) in THF (10 mL) was added $NaBH_4$ (1.2 mmol) in three portions. The reaction mixture was stirred at room temperature for 8 h under a N_2 atmosphere. The reaction mixture was quenched with H_2O (20 mL), extracted with CH_2Cl_2, and washed with water and brine. The organic layer was dried over Na_2SO_4 and concentrated in vacuo. The residue was purified by column chromatography to yield **25** (yield 80%). **10** was synthesized by general procedures A and D using **25** as the starting material (yield 41%). ^{1}H NMR (500 MHz, CD_3OD): δ 7.62 (dt, J = 7.5, 3.5 Hz, 2H), 7.58−7.51 (m, 2H), 7.37 (t, J = 7.5 Hz, 1H), 7.25 (t, J = 7.5 Hz, 1H), 7.20 (d, J = 7.5 Hz, 1H), 7.13−7.07 (m, 3H), 6.93 (dt, J = 7.5, 2.5 Hz, 1H), 6.69 (dd, J = 7.5, 2.5 Hz, 1H), 6.60−6.54 (m, 2H), 5.05−5.00 (m, 1H), 4.15−4.00 (m, 2H). ^{13}C NMR (125 MHz, CD_3OD): δ 161.37, 144.06, 131.34, 130.62, 129.88, 128.51, 128.38, 123.20, 122.77, 121.79, 116.23, 110.97, 110.09, 74.18, 73.46. LC-TOF (M + H^+) calcd for $C_{24}H_{23}N_4O_2S_2$ 463.1257, found 463.1256.

***N*,*N*′-((Ethane-1,2-diylbis(oxy))bis(3,1-phenylene))bis-(thiophene-2-carboximidamide) (11).** To a solution of 3-nitrophenol (2 mmol) in DMF (20 mL) was added K_2CO_3 (2.2 mmol) and 1,3-dibromopropane (1 mmol). The suspension was then stirred for 6 h at 60 °C. The reaction mixture was then diluted with H_2O (50 mL), extracted with EtOAc, and washed with water and brine. The organic layer was dried over Na_2SO_4 and concentrated in vacuo. The residue was purified by column chromatography to yield **27** (yield 80%). **11** was synthesized by general procedures A and D using **27** as the starting material (yield 59%). ^{1}H NMR (500 MHz, CD_3OD): δ 8.01 (t, J = 4.0 Hz, 4H), 7.47 (t, J = 8.0 Hz, 2H), 7.33 (t, J = 4.0 Hz, 2H), 7.03 (dd, J = 8.0, 2.0 Hz, 2H), 6.97 (t, J = 2.0 Hz, 2H), 6.94 (dd, J = 8.0, 2.0 Hz, 2H), 4.43 (s, 4H). ^{13}C NMR (125 MHz, CD_3OD): δ 161.52, 157.72, 133.75, 133.12, 132.15, 129.64, 129.49, 118.15, 114.83, 112.12, 68.12. LC-TOF (M + H^+) calcd for $C_{24}H_{23}N_4O_2S_2$ 463.1257, found 463.1257.

***N*,*N*′-((Propane-1,3-diylbis(oxy))bis(3,1-phenylene))bis-(thiophene-2-carboximidamide) (12).** **12** was synthesized by the same procedures as those to prepare **11** using 1,4-dibromobutane as the starting material. ^{1}H NMR (500 MHz, CD_3OD): δ 8.09−7.99 (m, 4H), 7.49 (t, J = 8.0 Hz, 2H), 7.41−7.33 (m, 2H), 7.11−7.05 (dd, J = 8.0, 2.5 Hz, 2H), 7.03 (t, J = 2.5 Hz, 2H), 7.00 (dd, J = 8.0, 2.5 Hz, 2H), 4.28 (t, J = 6.0 Hz, 4H), 2.33 (p, J = 6.0 Hz, 2H). ^{13}C NMR (125 MHz, CD_3OD): δ 161.77, 158.79, 146.61, 134.93, 134.51, 132.32, 129.83, 118.43, 115.89, 112.62, 65.88, 30.21. LC-TOF (M + H^+) calcd for $C_{25}H_{25}N_4O_2S_2$ 477.1413, found 477.1411.

***N*-(3-(2-((3-(Thiophene-2-carboximidamido)benzyl)amino)-ethyl)phenyl)thiophene-2-carboximidamide (13).** **13** was synthesized by general procedures B, C, A, D, and E using 3-nitrobenzaldehyde and 2-(3-nitrophenyl)ethanamine as the starting materials. ^{1}H NMR (500 MHz, CD_3OD): δ 7.65 (t, J = 5.0 Hz, 2H), 7.56 (dt, J = 5.0, 2.0 Hz, 2H), 7.38−7.27 (m, 2H), 7.17−7.09 (m, 2H), 7.06 (dt, J = 7.5, 1.5 Hz, 1H), 7.01−6.94 (m, 2H), 6.91 (dt, J = 7.5, 1.5 Hz, 1H), 6.88−6.82 (m, 2H), 3.79 (s, 2H), 2.96−2.81 (m, 4H). ^{13}C NMR (125 MHz, CD_3OD): δ 161.52, 153.94, 150.23, 142.53, 141.90, 141.06, 130.73, 130.67, 129.87, 129.83, 128.49, 128.39, 125.03, 124.76, 123.95, 123.69, 122.60, 121.58, 54.30, 51.28, 36.59. LC-TOF (M + H^+) calcd for $C_{25}H_{26}N_5S_2$ 460.1624, found 460.1618.

***N*-(4-(2-((3-(Thiophene-2-carboximidamido)benzyl)amino)-ethyl)phenyl)thiophene-2-carboximidamide (14).** **14** was synthesized by the same procedures as those to prepare **13** using 2-(4-nitrophenyl)ethanamine as the starting material. ^{1}H NMR (500 MHz, CD_3OD): δ 7.65−7.58 (m, 2H), 7.58−7.51 (m, 2H), 7.33 (t, J = 7.5 Hz, 1H), 7.24−7.17 (m, 2H), 7.13−7.07 (m, 2H), 7.04 (dt, J = 7.5, 2.0 Hz, 1H), 6.95 (t, J = 2.0 Hz, 1H), 6.93−6.85 (m, 3H), 3.84−3.70 (m, 2H), 2.93−2.74 (m, 4H). ^{13}C NMR (125 MHz, CD_3OD): δ 153.93, 141.90, 141.03, 136.14, 130.99, 130.86, 130.66, 130.30, 129.86, 129.80, 128.50, 128.44, 128.37, 124.76, 123.80, 123.66, 123.60, 122.61, 54.27, 51.49, 36.09. LC-TOF (M + H^+) calcd for $C_{25}H_{26}N_5S_2$ 460.1624, found 460.1620.

***N*-(4-(2-(Ethyl(3-(thiophene-2-carboximidamido)benzyl)-amino)ethyl)phenyl)thiophene-2-carboximidamide (15).** **35** was synthesized by general procedure B using 3-nitrobenzaldehyde and 2-(4-nitrophenyl)ethanamine as the starting materials. To a solution of **35** (1 mmol) and acetaldehyde (2 equiv) in THF (10 mL) was added $NaBH_4$ (1.2 mmol) in three portions. The reaction mixture was stirred at room temperature for 8 h under a N_2 atmosphere. The reaction mixture was then quenched with H_2O (20 mL), extracted with CH_2Cl_2, and washed with water and brine. The organic layer was dried over Na_2SO_4 and concentrated in vacuo. The residue was purified by column chromatography to yield **39** (yield 64%). **15** was synthesized by general procedures A and D using **39** as the starting material. ^{1}H NMR (500 MHz, CD_3OD): δ 7.69−7.60 (m, 2H), 7.60−7.54 (m, 2H), 7.36 (t, J = 7.5 Hz, 1H), 7.24−7.17 (m, 2H), 7.14−7.09 (m, 3H), 7.05−6.99 (m, 1H), 6.96−6.87 (m, 3H), 3.72 (s, 2H), 2.88−2.73 (m, 4H), 2.72−2.64 (q, J = 7.0 Hz, 2H), 1.16 (t, J = 7.0 Hz, 3H). ^{13}C NMR (125 MHz, CD_3OD): δ 150.04, 141.15, 141.01, 136.83, 130.90, 130.43, 129.86, 129.79, 128.43, 128.37, 128.35, 125.79, 124.76, 123.65, 122.58, 58.73, 55.97, 33.01, 11.75. LC-TOF (M + H^+) calcd for $C_{27}H_{30}N_5S_2$ 488.1937, found 488.1932.

***N*-(3-(((3-Fluorophenethyl)amino)methyl)phenyl)thiophene-2-carboximidamide (16).** **16** was synthesized by the same procedures as those to prepare **13** using 3-fluorobenzaldehyde as the starting material. ^{1}H NMR (400 MHz, CD_3OD): δ 8.18−8.04 (m, 2H), 7.81−7.69 (m, 2H), 7.65 (t, J = 7.5 Hz, 1H), 7.58−7.50 (m, 1H), 7.41−7.28 (m, 2H), 7.18−7.06 (m, 2H), 7.03−6.93 (m, 1H), 4.37 (s, 2H), 3.42−3.31 (m, 2H), 3.20−3.10 (m, 2H). ^{13}C NMR (100 MHz, CD_3OD): δ 164.17, 161.74 (s), 139.31 (d, J = 7.5 Hz), 134.72, 134.45, 134.22, 133.50, 130.87, 130.55, 130.34 (d, J = 7.5 Hz), 128.66, 127.22, 126.47, 124.49, 124.46, 115.30 (d, J = 20 Hz), 113.56 (d, J = 20 Hz), 109.99, 50.38, 48.27, 31.49 (d, J = 2.0 Hz). LC-TOF (M + H^+) calcd for $C_{20}H_{21}FN_3S$ 354.1435, found 354.1441.

***N*-(3-((Ethyl(3-fluorophenethyl)amino)methyl)phenyl)-thiophene-2-carboximidamide (17).** **17** was synthesized by the same procedures as those to prepare **15** using 3-fluorobenzaldehyde

dx.doi.org/10.1021/jm401252e | J. Med. Chem. 2014, 57, 686−700

Table 5. Crystallographic Data Collection and Refinement Statistics

data set[a]	nNOS-7	nNOS-9	nNOS-11	nNOS-13
Data Collection				
PDB code	4KCH	4KCI	4KCJ	4KCK
space group	$P2_12_12_1$	$P2_12_12_1$	$P2_12_12_1$	$P2_12_12_1$
cell dimensions *a*, *b*, *c* (Å)	51.7, 111.6, 165.0	51.8, 111.9, 165.0	51.8, 110.0, 164.7	51.9, 111.0, 165.3
resolution (Å)	2.15 (2.19−2.15)	2.27 (2.31−2.27)	2.05 (2.09−2.05)	2.10 (2.14−2.10)
R_{merge}	0.066 (0.559)	0.055 (0.677)	0.055 (0.799)	0.069 (0.720)
$I/\sigma I$	20.0 (1.3)	29.7 (1.9)	25.1 (2.1)	20.7 (1.5)
no. unique reflns	52573	44477	61070	52371
completeness (%)	99.4 (98.1)	98.3 (97.8)	99.6 (97.8)	92.6 (100.0)
redundancy	3.6 (3.6)	4.0 (4.2)	3.6 (3.4)	3.5 (3.7)
Refinement				
resolution (Å)	2.15	2.27	2.05	2.10
no. reflns used	49887	42147	57366	49419
R_{work}/R_{free}[b]	0.194/0.250	0.181/0.238	0.195/0.242	0.216/0.264
no. atoms				
protein	6659	6659	6665	6681
ligand/ion	185	189	193	179
water	167	122	259	379
RMS deviations				
bond lengths (Å)	0.011	0.016	0.013	0.012
bond angles (deg)	2.02	2.27	2.11	2.10
data set[a]	nNOS-14	nNOS-15	nNOS-16	nNOS-17
Data Collection				
PDB code	4KCL	4KCM	4KCN	4KCO
space group	$P2_12_12_1$	$P2_12_12_1$	$P2_12_12_1$	$P2_12_12_1$
cell dimensions *a*, *b*, *c* (Å)	52.1, 111.1, 165.1	51.7, 110.8, 165.2	52.1, 111.0, 165.0	52.0, 110.9, 165.0
resolution (Å)	1.93 (1.96−1.93)	2.08 (2.12−2.08)	1.85 (1.88−1.85)	1.86 (1.89−1.86)
R_{merge}	0.057 (0.479)	0.068 (0.762)	0.050 (0.660)	0.057 (0.680)
$I/\sigma I$	26.3 (2.1)	23.1 (1.7)	29.2 (2.6)	28.2 (2.1)
no. unique reflns	71898	58123	82346	81114
completeness (%)	98.0 (97.8)	99.6 (100.0)	99.3 (99.9)	99.4 (100.0)
redundancy	3.3 (3.2)	3.8 (3.8)	4.0 (4.1)	3.9 (3.8)
Refinement				
resolution (Å)	2.10	2.07	1.85	1.86
no. reflns used	68,060	55,146	77,959	76,678
R_{work}/R_{free}[b]	0.182/0.213	0.191/0.236	0.185/0.217	0.187/0.220
no. atoms				
protein	6666	6668	6677	6685
ligand/ion	195	188	219	177
water	341	224	397	380
RMS deviations				
bond lengths (Å)	0.011	0.011	0.012	0.014
bond angles (deg)	1.45	2.05	1.52	1.62
data set[a]	eNOS-14	eNOS-15	eNOS-16	eNOS-17
Data Collection				
PDB code	4KCP	4KCQ	4KCR	4KCS
space group	$P2_12_12_1$	$P2_12_12_1$	$P2_12_12_1$	$P2_12_12_1$
cell dimensions *a*, *b*, *c* (Å)	57.7, 106.2, 156.8	57.7, 106.4, 156.7	57.6, 106.2, 156.5	57.7, 106.4, 157.1
resolution (Å)	2.07 (2.11−2.07)	2.03 (2.07−2.03)	2.09 (2.13−2.09)	2.05 (2.09−2.05)
R_{merge}	0.060 (0.712)	0.064 (0.494)	0.059 (0.576)	0.051 (0.528)
$I/\sigma I$	24.2 (1.9)	26.9 (2.6)	27.3 (2.6)	31.0 (2.9)
no. unique reflns	59332	62254	57743	61246
Completeness (%)	99.1 (99.9)	98.4 (99.7)	99.7 (100.0)	99.2 (100.0)
Redundancy	4.0 (4.0)	3.9 (3.9)	4.0 (4.1)	4.0 (4.0)
Refinement				
Resolution (Å)	2.07	2.03	2.09	2.05
No. reflns used	56198	59095	54719	58050
R_{work}/R_{free}[b]	0.166/0.213	0.179/0.224	0.164/0.205	0.168/0.213
No. atoms				
protein	6446	6429	6436	6446

dx.doi.org/10.1021/jm401252e | J. Med. Chem. 2014, 57, 686−700

Table 5. continued

data set[a]	eNOS-14	eNOS-15	eNOS-16	eNOS-17
Refinement				
ligand/ion	216	223	206	201
water	305	359	354	350
RMS deviations				
bond lengths (Å)	0.020	0.013	0.011	0.020
bond angles (deg)	2.02	1.63	1.45	2.05

[a]See Figure 3 for the inhibitor chemical structure. [b]R_{free} was calculated with the 5% of reflections set aside throughout the refinement. The set of reflections for the R_{free} calculation were kept the same for all data sets of each isoform according to those used in the data of the starting model.

and 2-(3-nitrophenyl)ethanamine as the starting materials. ^{1}H NMR (400 MHz, CD_3OD): δ 7.85−7.72 (m, 2H), 7.43 (t, J = 7.5 Hz, 1H), 7.31−7.17 (m, 4H), 7.12 (dt, J = 7.5, 1.0 Hz, 1H), 7.02 (dt, J = 7.5, 1.0 Hz, 1H), 6.97 (dt, J = 9.0, 2.5 Hz, 1H), 6.88 (td, J = 9.0, 2.5 Hz, 1H), 3.96 (s, 2H), 2.99−2.82 (m, 6H), 1.18 (t, J = 7.0 Hz, 3H). ^{13}C NMR (100 MHz, CD_3OD): δ 164.05, 161.62, 141.73 (d, J = 7.5 Hz), 135.05, 130.92, 130.00, 129.91, 129.82, 129.80, 127.70, 126.86, 124.80, 124.44, 124.41, 123.27, 115.19 (d, J = 20 Hz), 112.72 (d, J = 20 Hz), 109.99, 56.82, 53.51, 47.10, 31.10, 9.67. LC-TOF ($M + H^+$) calcd for $C_{22}H_{25}FN_3S$ 382.1748, found 382.1742.

Enzyme Assays. The three isozymes, rat nNOS, murine macrophage iNOS, and bovine eNOS, were recombinant enzymes, overexpressed (in *Escherichia coli*) and isolated as reported.[28−30] K_i values for inhibitors **7**−**17** were measured for the three different isoforms of NOS using L-arginine as a substrate. The formation of nitric oxide was measured using the hemoglobin capture assay described previously.[31] All NOS isozymes were assayed using the Synergy H1 hybrid multimode microplate reader (BioTek Instruments, Inc.) at 37 °C in a 100 mM Hepes buffer (pH 7.4) containing 10 μM L-arginine, 0.83 mM $CaCl_2$, 320 units/mL calmodulin, 100 μM NADPH, 10 μM H_4B, and 3.0 μM oxyhemoglobin (for iNOS assays, no Ca^{2+} and calmodulin was added). The assay was initiated by the addition of enzyme, and the initial rates of the enzymatic reactions were determined by monitoring the formation of NO−hemoglobin complex at 401 nm for 60 s. The apparent K_i values were obtained by measuring the percent enzyme inhibition in the presence of 10 μM L-arginine with at least five concentrations of inhibitor. The parameters of the following inhibition equation were fitted to the initial velocity data: % inhibition = $100[I]/\{[I] + K_i(1 + [S]/K_m)\}$. K_m values for L-arginine were 1.3 μM (nNOS), 8.2 μM (iNOS), and 1.7 μM (eNOS). The selectivity of an inhibitor was defined as the ratio of the respective K_i values.

Inhibitor Complex Crystal Preparation. The nNOS or eNOS heme domain proteins used for crystallographic studies were produced by limited trypsin digest from the corresponding full length enzymes and further purified through a Superdex 200 gel filtration column (GE Healthcare) as described previously.[32,33] The nNOS heme domain at 7−9 mg/mL containing 20 mM histidine or the eNOS heme domain at 12 mg/mL containing 2 mM imidazole were used for the sitting drop vapor diffusion crystallization setup under the conditions reported before.[32,33] Fresh crystals (1−2 day old) were first passed stepwise through cryoprotectant solutions as described[32,33] and then soaked with 10 mM inhibitor for 4−6 h at 4 °C before being mounted on nylon loops and flash cooled by plunging into liquid nitrogen.

X-ray Diffraction Data Collection, Processing, and Structure Refinement. The cryogenic (100 K) X-ray diffraction data were collected remotely at various beamlines at Stanford Synchrotron Radiation Lightsource through the data collection control software Blu-Ice[34] and a crystal mounting robot. Raw data frames were indexed, integrated, and scaled using HKL2000.[35] The binding of inhibitors was detected by the initial difference Fourier maps calculated with REFMAC.[36] The inhibitor molecules were then modeled in COOT[37] and refined using REFMAC. Disordering in portions of inhibitor bound in the NOS active site was often observed, resulting in poor density quality. However, partial structural features usually could still be visible if the contour level of the sigmaA weighted $2m|F_o| - D|F_c|$ map dropped to 0.5 σ, which afforded building of a reasonable model into the disordered regions. Water molecules were added in REFMAC and checked by COOT. The TLS[38] protocol was implemented in the final stage of refinements with each subunit as one TLS group. The omit $F_o - F_c$ density maps were calculated by repeating the last round of TLS refinement with inhibitor coordinate removed from the input PDB file to generate the coefficients DELFWT and SIGDELFWT. The refined structures were validated in COOT before deposition in the RCSB Protein Data Bank. The crystallographic data collection and structure refinement statistics are summarized in Table 5 with PDB accession codes included.

■ ASSOCIATED CONTENT

Supporting Information

Details of HPLC purity and copies of complete spectroscopic data of compounds **7**−**17**. This material is available free of charge via the Internet at http://pubs.acs.org.

■ AUTHOR INFORMATION

Corresponding Authors

*For R.B.S.: phone, +1 847 491 5653; fax, +1 847 491 7713; E-mail, Agman@chem.northwestern.edu.

*For T.L.P.: phone, +1 949 824 7020; E-mail, poulos@uci.edu.

Notes

The authors declare no competing financial interest.

■ ACKNOWLEDGMENTS

We are grateful for financial support from the National Institutes of Health (GM049725 to R.B.S. and GM057353 to T.L.P.). We thank Dr. Bettie Sue Siler Masters (NIH grant GM52419, with whose laboratory P.M. and L.J.R. are affiliated). B.S.S.M. also acknowledges the Welch Foundation for a Robert A. Welch Distinguished Professorship in Chemistry (AQ0012). P.M. is supported by grants 0021620806 and 1M0520 from MSMT of the Czech Republic. We also thank the beamline staff at SSRL and ALS for their assistance during the remote X-ray diffraction data collections.

■ ABBREVIATIONS USED

NOS, nitric oxide synthase; NO, nitric oxide; NADPH, reduced nicotinamide adenine dinucleotide phosphate; NHA, N^{ω}-hydroxy-L-arginine; nNOS, neuronal nitric oxide synthase; eNOS, endothelial nitric oxide synthase; iNOS, inducible nitric oxide synthase; H-bond, hydrogen bond

■ REFERENCES

(1) Calabrese, V.; Mancuso, C.; Calvani, M.; Rizzarelli, E.; Butterfield, D. A.; Stella, A. M. G. Nitric oxide in the central nervous system: neuroprotection versus neurotoxicity. *Nature Rev. Neurosci.* **2007**, *8*, 766−775.

(2) Rosen, G. M.; Tsai, P.; Pou, S. Mechanism of free-radical generation by nitric oxide synthase. *Chem. Rev.* **2002**, *102*, 1191−1199.

(3) Griffith, O. W.; Stuehr, D. J. Nitric Oxide Synthases: Properties and Catalytic Mechanism. *Annu. Rev. Physiol.* **1995**, *57*, 707−734.
(4) Granik, V. G.; Grigor'ev, N. A. Nitric oxide synthase inhibitors: biology and chemistry. *Russ. Chem. Bull.* **2002**, *51*, 1973−1995.
(5) Alderton, W. K.; Cooper, C. E.; Knowles, R. G. Nitric oxide synthases: structure, function and inhibition. *Biochem. J.* **2001**, *357*, 593−615.
(6) Vallance, P.; Leiper, J. Blocking NO synthesis: How, where and why? *Nature Rev. Drug Discovery* **2002**, *1*, 939−950.
(7) Yang, Z.; Misner, B.; Ji, H.; Poulos, T. L.; Silverman, R. B.; Meyskens, F. L.; Yang, S. Targeting Nitric Oxide Signaling with nNOS Inhibitors As a Novel Strategy for the Therapy and Prevention of Human Melanoma. *Antioxid. Redox Signaling* **2013**, *19*, 433−447.
(8) Villanueva, C.; Giulivi, C. Subcellular and cellular locations of nitric oxide synthase isoforms as determinants of health and disease. *Free Radical Biol. Med.* **2010**, *49*, 307−316.
(9) Olesen, J. Nitric oxide-related drug targets in headache. *Neurotherapeutics* **2010**, *7*, 183−190.
(10) Li, H.; Shimizu, H.; Flinspach, M.; Jamal, J.; Yang, W.; Xian, M.; Cai, T.; Wen, E. Z.; Jia, Q.; Wang, P. G.; Poulos, T. L. The Novel Binding Mode of *N*-Alkyl-*N*′-hydroxyguanidine to Neuronal Nitric Oxide Synthase Provides Mechanistic Insights into NO Biosynthesis. *Biochemistry* **2002**, *41*, 13868−13875.
(11) Masic, L. P. Arginine mimetic structures in biologically active antagonists and inhibitors. *Curr. Med. Chem.* **2006**, *13*, 3627−3648.
(12) Silverman, R. B. Design of selective neuronal nitric oxide synthase inhibitors for the prevention and treatment of neurodegenerative diseases. *Acc. Chem. Res.* **2009**, *42*, 439−451.
(13) Delker, S. L.; Ji, H.; Li, H..; Jamal, J.; Fang, J.; Xue, F.; Silverman, R. B.; Poulos, T. L. Unexpected binding modes of nitric oxide synthase inhibitors effective in the prevention of a cerebral palsy phenotype in an animal model. *J. Am. Chem. Soc.* **2010**, *132*, 5437−5442.
(14) Ji, H.; Li, H.; Martasek, P.; Roman, L. J.; Poulos, T. L.; Silverman, R. B. Discovery of highly potent and selective inhibitors of neuronal nitric oxide synthase by fragment hopping. *J. Med. Chem.* **2009**, *52*, 779−797.
(15) Ji, H.; Delker, S. L.; Li, H.; Martasek, P.; Roman, L. J.; Poulos, T. L.; Silverman, R. B. Exploration of the active site of neuronal nitric oxide synthase by the design and synthesis of pyrrolidinomethyl 2-aminopyridine derivatives. *J. Med. Chem.* **2010**, *53*, 7804−7824.
(16) Huang, H.; Ji, H.; Li, H.; Jing, Q.; Jansen Labby, K.; Martasek, P.; Roman, L. J.; Poulos, T. L.; Silverman, R. B. Selective monocationic inhibitors of neuronal nitric oxide synthase. Binding mode insights from molecular dynamics simulations. *J. Am. Chem. Soc.* **2012**, *134*, 11559−11572.
(17) Xue, F.; Fang, J.; Delker, S. L.; Li, H.; Martasek, P.; Roman, L. J.; Poulos, T. L.; Silverman, R. B. Symmetric double-headed aminopyridines, a novel strategy for potent and membrane-permeable inhibitors of neuronal nitric oxide synthase. *J. Med. Chem.* **2011**, *54*, 2039−2048.
(18) Huang, H.; Li, H.; Martásek, P.; Roman, L. J.; Poulos, T. L.; Silverman, R. B. Structure-guided design of selective inhibitors of neuronal nitric oxide synthase. *J. Med. Chem.* **2013**, *56*, 3024−3032.
(19) Jansen Labby, K.; Xue, F.; Kraus, J. M.; Ji, H.; Mataka, J.; Li, H.; Martasek, P.; Roman, L. J.; Poulos, T. L.; Silverman, R. B. Intramolecular hydrogen bonding: a potential strategy for more bioavailable inhibitors of neuronal nitric oxide synthase. *Bioorg. Med. Chem.* **2012**, *20*, 2435−2443.
(20) Ramnauth, J.; Speed, J.; Maddaford, S. P.; Dove, P.; Annedi, S. C.; Renton, P.; Rakhit, S.; Andrews, J.; Silverman, S.; Mladenova, G.; Zinghini, S.; Nair, S.; Catalano, C.; Lee, D. K.; De Felice, M.; Porreca, F. Design, synthesis, and biological evaluation of 3,4-dihydroquinolin-2(1*H*)-one and 1,2,3,4-tetrahydroquinoline-based selective human neuronal nitric oxide synthase (nNOS) inhibitors. *J. Med. Chem.* **2011**, *54*, 5562−5575.
(21) Ramnauth, J.; Renton, P.; Dove, P.; Annedi, S. C.; Speed, J.; Silverman, S.; Mladenova, G.; Maddaford, S. P.; Zinghini, S.; Rakhit, S.; Andrews, J.; Lee, D. K.; Zhang, D.; Porreca, F. 1,2,3,4-Tetrahydroquinoline-based selective human neuronal nitric oxide synthase (nNOS) inhibitors: lead optimization studies resulting in the identification of *N*-(1-(2-(methylamino)ethyl)-1,2,3,4-tetrahydroquinolin-6-yl)thiophene-2-carboximi damide as a preclinical development candidate. *J. Med. Chem.* **2012**, *55*, 2882−2893.
(22) Annedi, S. C.; Ramnauth, J.; Cossette, M.; Maddaford, S. P.; Dove, P.; Rakhit, S.; Andrews, J. S.; Porreca, F. Novel, druglike 1,7-disubstituted 2,3,4,5-tetrahydro-1*H*-benzo[*b*]azepine-based selective inhibitors of human neuronal nitric oxide synthase (nNOS). *Bioorg. Med. Chem. Lett.* **2012**, *22*, 2510−2513.
(23) Renton, P.; Speed, J.; Maddaford, S.; Annedi, S. C.; Ramnauth, J.; Rakhit, S.; Andrews, J. 1,5-Disubstituted indole derivatives as selective human neuronal nitric oxide synthase inhibitors. *Bioorg. Med. Chem. Lett.* **2011**, *21*, 5301−5304.
(24) Annedi, S. C.; Maddaford, S. P.; Mladenova, G.; Ramnauth, J.; Rakhit, S.; Andrews, J. S.; Lee, D. K. H.; Zhang, D. Q.; Porreca, F.; Bunton, D.; Christie, L. Discovery of *N*-(3-(1-methyl-1,2,3,6-tetrahydropyridin-4-yl)-1*H*-indol-6-yl) thiophene-2-carboximidamide as a selective inhibitor of human neuronal nitric oxide synthase (nNOS) for the treatment of pain. *J. Med. Chem.* **2011**, *54*, 7408−7416.
(25) Mladenova, G.; Annedi, S. C.; Ramnauth, J.; Maddaford, S. P.; Rakhit, S.; Andrews, J. S.; Zhang, D. Q.; Porreca, F. First-in-class, dual-action, 3,5-disubstituted indole derivatives having human nitric oxide synthase (nNOS) and norepinephrine reuptake inhibitory (NERI) activity for the treatment of neuropathic pain. *J. Med. Chem.* **2012**, *55*, 3488−3501.
(26) Ziegler, D. M.; Ansher, S. S.; Nagata, T.; Kadlubar, F. F.; Jakoby, W. B. *N*-Methylation: potential mechanism for metabolic activation of carcinogenic primary arylamines. *Proc. Natl. Acad. Sci. U. S. A.* **1988**, *85*, 2514−2517.
(27) Hodgetts, K. J.; Combs, K. J.; Elder, A. M.; Harriman, G. C. The Role of Fluorine in the Discovery and Optimization of CNS Agents: Modulation of Drug-Like Properties. *Annu. Rep. Med. Chem.* **2010**, *45*, 429−448.
(28) Hevel, J. M.; White, K. A.; Marletta, M. A. Purification of the inducible murine macrophage nitric oxide synthase. Identification as a flavoprotein. *J. Biol. Chem.* **1991**, *266*, 22789−22791.
(29) Roman, L. J.; Sheta, E. A.; Martasek, P.; Gross, S. S.; Liu, Q.; Masters, B. S. S. High-level expression of functional rat neuronal nitric oxide synthase in *Escherichia coli*. *Proc. Natl. Acad. Sci. U. S. A.* **1995**, *92*, 8428−8432.
(30) Martasek, P.; Liu, Q.; Liu, J. W.; Roman, L. J.; Gross, S. S.; Sessa, W. C.; Masters, B. S. S. Characterization of Bovine Endothelial Nitric Oxide Synthase Expressed in *E. coli*. *Biochem. Biophys. Res. Commun.* **1996**, *219*, 359−365.
(31) Hevel, J. M.; Marletta, M. A. Nitric-oxide synthase assays. In *Oxygen Radicals in Biological Systems, Part C*; Methods in Enzymology; Academic Press: San Diego, CA, 1994; Vol. *233*, pp 250−258.
(32) Li, H.; Shimizu, H.; Flinspach, M.; Jamal, J.; Yang, W.; Xian, M.; Cai, T.; Wen, E. Z.; Jia, Q.; Wang, P. G.; Poulos, T. L. The Novel Binding Mode of *N*-Alkyl-*N*′-hydroxyguanidine to Neuronal Nitric Oxide Synthase Provides Mechanistic Insights into NO Biosynthesis. *Biochemistry* **2002**, *41*, 13868−13875.
(33) Raman, C. S.; Li, H.; Martásek, P.; Král, V.; Masters, B. B. S.; Poulos, T. L. Crystal structure of constitutive endothelial nitric oxide synthase: a paradigm for pterin function involving a novel metal center. *Cell* **1998**, *95*, 939−950.
(34) McPhillips, T. M.; McPhillips, S. E.; Chiu, H. J.; Cohen, A. E.; Deacon, A. M.; Ellis, P. J.; Garman, E.; Gonzalez, A.; Sauter, N. K.; Phizackerley, R. P.; Soltis, S. M.; Kuhn, P. Blu-Ice and the Distributed Control System: Software for Data Acquisition and Instrument Control at Macromolecular Crystallography Beamlines. *J. Synchrotron Radiat.* **2002**, *9*, 401−406.
(35) Otwinowski, Z.; Minor, W. Processing of X-ray Diffraction Data Collected in Oscillation Mode. *Methods Enzymol.* **1997**, *276*, 307−326.
(36) Murshudov, G. N.; Vagin, A. A.; Dodson, E. J. Refinement of Macromolecular Structures by the Maximum-Likelihood Method. *Acta Crystallogr., Sect. D: Biol. Crystallogr.* **1997**, *D53*, 240−255.

(37) Emsley, P.; Cowtan, K. Coot: model-building tools for molecular graphics. *Acta Crystallogr., Sect. D: Biol. Crystallogr.* **2004**, *D60*, 2126−2132.
(38) Winn, M. D.; Isupov, M. N.; Murshudov, G. N. Use of TLS Parameters to Model Anisotropic Displacements in Macromolecular Refinement. *Acta Crystallogr., Sect. D: Biol. Crystallogr.* **2001**, *D57*, 122−133.
(39) Patman, J.; Bhardwaj, N.; Ramnauth, J.; Annedi, S. C.; Renton, P.; Maddaford, S. P.; Rakhit, S.; Andrews, J. S. Novel 2-amino-benzothiazoles as selective neuronal nitric oxide synthase inhibitors. *Bioorg. Med. Chem. Lett.* **2007**, *17*, 2540−2544.